

The transport properties of Dirac fermions in chemical vapour-deposited single-layer graphene

Engin Arslan, Şükrü Ardalı, Engin Tıraş, Semih Çakmakyapan & Ekmel Özbay

To cite this article: Engin Arslan, Şükrü Ardalı, Engin Tıraş, Semih Çakmakyapan & Ekmel Özbay (2017) The transport properties of Dirac fermions in chemical vapour-deposited single-layer graphene, Philosophical Magazine, 97:3, 187-200, DOI: [10.1080/14786435.2016.1247994](https://doi.org/10.1080/14786435.2016.1247994)

To link to this article: <http://dx.doi.org/10.1080/14786435.2016.1247994>



Published online: 24 Oct 2016.



Submit your article to this journal [↗](#)



Article views: 93



View related articles [↗](#)



View Crossmark data [↗](#)

The transport properties of Dirac fermions in chemical vapour-deposited single-layer graphene

Engin Arslan^a, Şükrü Ardalı^b, Engin Tıraş^b, Semih Çakmakyapan^c and Ekmel Özbay^{a,d}

^aDepartment of Physics, Nanotechnology Research Center-NANOTAM, Bilkent University, Ankara, Turkey;

^bFaculty of Science, Department of Physics, Anadolu University, Eskisehir, Turkey; ^cElectrical Engineering Department, University of California, Los Angeles, CA, USA; ^dDepartment of Electrical and Electronics Engineering, Bilkent University, Ankara, Turkey

ABSTRACT

The electronic transport properties of Dirac fermions in chemical vapour-deposited single-layer epitaxial graphene on anSiO₂/Si substrate have been investigated using the Shubnikov–de Haas (SdH) oscillations technique. The magnetoresistance measurements were performed in the temperature range between 1.8 and 43 K and at magnetic fields up to 11 T. The 2D carrier density and the Fermi energy have been determined from the period of the SdH oscillations. In addition, the in-plane effective mass as well as the quantum lifetime of 2D carriers have been calculated from the temperature and magnetic field dependences of the SdH oscillation amplitude. The sheet carrier density ($1.42 \times 10^{13} \text{ cm}^{-2}$ at 1.8 K), obtained from the low-field Hall Effect measurements, is larger than that of 2D carrier density ($8.13 \times 10^{12} \text{ cm}^{-2}$). On the other hand, the magnetoresistance includes strong magnetic field dependent positive, non-oscillatory background magnetoresistance. The strong magnetic field dependence of the magnetoresistance and the differences between sheet carrier and 2D carrier density can be attributed to the 3D carriers between the graphene sheet and the SiO₂/Si substrate.

ARTICLE HISTORY

Received 3 August 2015
Accepted 6 October 2016

KEYWORDS

B1.Graphene; A1.SdH oscillations; A1.Hall effect

1. Introduction

Because of its exceptional properties, including ballistic transport, high current density, high thermal conductivity, chemical inertness, optical transmittance and super hydrophobicity at the nanometer scale, graphene, a one-atom-thick planar sheet of sp²-bonded carbon atoms densely packed in a honeycomb crystal lattice [1–4], has been attracting interest for applications such as solar cells, light-emitting devices, touch screens, photodetectors, ultrafast lasers, membranes, spin valves and high-frequency electronics[5–7].

Different methods are used for graphene synthesis [8]. The first success in the synthesis of monolayer graphene was made by the group of Geim and Novoselov using mechanical exfoliation from bulk graphite [1]. The other mostly used methods are based on the thermal graphitisation of an SiC surface and by chemical vapour deposition (CVD) using a metallic

catalyst such as Ni, Cu and Ru [6]. The usages of the graphene in the device applications require the growth of a single- or multi-layer graphene on a suitable substrate. A detailed understanding of the carrier transport properties and scattering mechanisms of a graphene sheet is very important because the material is a potential candidate for being incorporated into the future generation of nano-electronic and nano-photonics devices [3,4,6].

The transport properties of graphene were studied both theoretically [9–11] and experimentally [12–19]. Tıraş et al. [16] published Shubnikov–de Haas (SdH) measurement results for single-layer graphene on a SiC substrate. They calculate the electronic properties, such as sheet carrier density, 2D carrier density, in-plane effective mass, quantum lifetimes and power loss for single-layer graphene from the SdH oscillations. Zou et al. [14] reported SdH measurement results for bilayer graphene on SiO₂/Si substrate. They calculated the effective mass both for the 2D hole and 2D electron gas for a wide range of carrier densities using SdH oscillations. In the study of Hong et al. [13], they published the results for the transport lifetime and the quantum lifetime in the single-layer graphene sheets that mechanically exfoliated onto SiO₂/Si substrates using SdH measurements, and suggested carrier mobility limiting scattering mechanisms. However, up to now, there have been no published experimental results for the transport properties that are determined by SdH measurement in single-layer CVD graphene (SLG) on SiO₂/Si substrate.

The purpose of the present paper is to study the transport properties of the SLG sheet on SiO₂/Si substrate. We present the results of the SdH effect and low-field Hall Effect measurements in p-doped single-layer graphene on a SiO₂/Si substrate. The sheet carrier density, 2D carrier density, in-plane effective mass, quantum lifetimes of 2D hole gas in a single-layer graphene sheet were determined experimentally. A strong magnetic field dependence of the magnetoresistance results was observed. This behaviour was attributed to the parallel conduction in the SLG/SiO₂/Si sample. In the case of single graphene sheet on an SiO₂/Si substrate, we have a degenerate high-mobility 2D hole gas in single-layer graphene with a much lower mobility 3D hole gas between the graphene sheet and SiO₂/Si substrate.

2. Samples preparation and measurement details

In the present study, SLG, which was grown on thin-film copper and subsequently transferred to an SiO₂ (285 nm)/Si substrate, was used. The graphene wafers were lithographed by conventional electron-beam lithography into Hall bar geometry with the length and width of $L = 1000 \mu\text{m}$ and $w = 500 \mu\text{m}$, respectively (Figure 1(a)). The 20 nm titanium and 100 nm gold were deposited by an electron beam evaporator, and then followed with the standard lift-off process. The mesa lithography step was performed in order to preserve the active graphene region, while etching the rest of the graphene on the surface with O₂ plasma. Interconnect metal lithography was performed using 30/220 nm Ti/Au metal pair. Finally, devices were bonded for measurements.

The layer number of the graphene sample was identified by Raman spectroscopy. Raman spectra were collected by the Jobin Yvon Horiba Raman Spectrometer system at room temperature. As an excitation source, a wavelength of 532 nm (2.33 eV) from a He–Ne excitation laser was applied. The data were collected with a 100X objective with 0.9 numerical apertures. A slit size of 200 μm and a hole size of 1100 μm was used throughout the measurements. The magnetoresistance (R_{xx}) measurements were performed using DC techniques under a static magnetic field up to 11 T in the temperature range from 1.8 to 43 K in

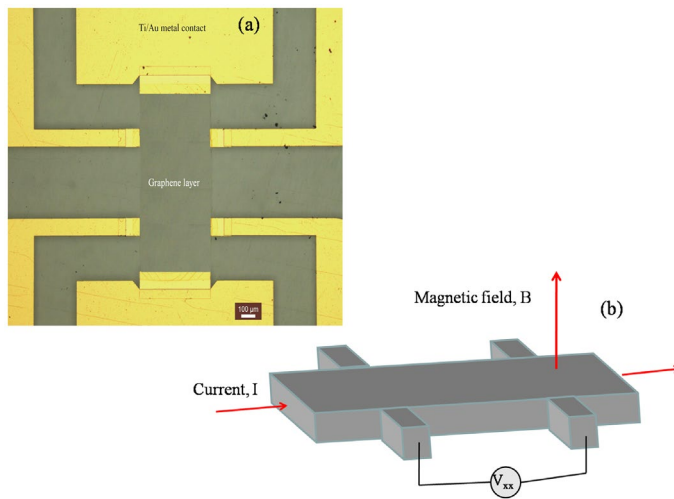


Figure 1. (colour online) (a) Optical image and (b) schematic diagram of the Hall-bar device patterned on an SLG/SiO₂/Si sample.

the cryogen free superconducting magnet system (Cryogenics Ltd., Model No. J2414) with combination of a constant current source (Keithley 2400) and a nanovoltmeter (Keithley 2182A). The current flow was in the plane of the 2D electron gas, and the current (100 μ A) through the sample was kept low enough to ensure ohmic conditions. Magnetic fields (B) were applied perpendicular to the plane of the samples. In order to calculate the sheet carrier density and Hall mobility as a function temperature, the R_{xx} and Hall resistance (R_{xy}) were measured as a function of temperature from 1.8 to 260 K under the static magnetic field of 1 T.

3. Results and discussion

3.1. Raman measurement

Raman spectroscopy is known to be a powerful tool used to probe the phonon spectrum of graphene. The Raman spectroscopy of graphene can be used to determine the number of graphene layers and stacking order as well as the density of the defects and impurities [20,21]. The Raman spectra exhibit a relatively simple structure characterised by two principle bands designated as the G and 2D bands, including a third band D that may also be apparent in spectra when defects within the carbon lattice are present [20,21]. The G band is a sharp band that appears around 1580 cm^{-1} in the spectrum of graphene [20,21]. The G band position is highly sensitive to the number of layers present in the sample and is one method for determining layer thickness and is based upon the observed position of this band for a sample [20,21]. The D band is known as the disorder-induced band or the defect band. The intensity of the D band is directly proportional to the level of defects in the sample [20,21]. The 2D band is the second order of the D band, sometimes called the overtone of the D band. Recently, they have demonstrated that the shape of the 2D Raman peak may serve as the fingerprint to distinguish mono-, bi- and few-layer graphene [20,21]. In contrast to the G band position, the 2D band method depends not only on the peak position but also

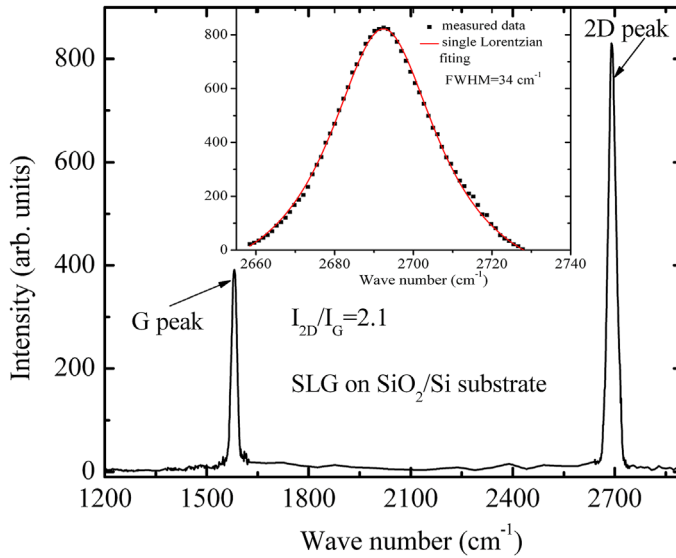


Figure 2. (colour online) Raman spectra of single-layer graphene on SiO_2/Si substrate.

on the band shape. The band shapes changes with graphene layer number [20]. For single layer graphene, the 2D band shape is seen as single symmetric peak and can be fitted to a single Lorentzian. With the increasing number of layers, the 2D band splits into several overlapping modes and requires fitting to two or more Lorentzians. The layer number of the graphene can also be determined by the peak intensity ratio of the 2D and G bands.

The Raman spectrum of the graphene layer on SiO_2/Si substrate is shown in Figure 2. The Raman spectrum of sample shows 2D peak around 2691 cm^{-1} . We find that the 2D band is well fitted with a single Lorentzian (inset of Figure 2) with a full with half maximum of 34 cm^{-1} . The G band position was also observed at 1588 cm^{-1} . On the other hand, Figure 2 shows that no disorder related *D* peak is observed in the graphene layers. This proves the absence of a significant number of defects. On the other hand, the peak intensity ratio of the 2D and G bands was calculated as 2.1 in our graphene layer on the SiO_2/Si sample. The I_{2D}/I_G ratio, observation of G peak at 1588 cm^{-1} , sharp symmetric 2D peak and lack of *D* peak are the confirmation for a high-quality defect-free single-layer graphene sample.

3.2. Hall mobility and sheet carrier density

The temperature dependent behaviour of the Hall mobility (μ_H) and the sheet carrier density (N_s) of carriers was determined from the measured R_{xx} and R_{xy} using equation [16,18];

$$\mu_H = \frac{L}{w} \frac{R_{xy}}{BR_{xx}} \quad (1)$$

$$N_s = \frac{B}{R_{xy}e} \quad (2)$$

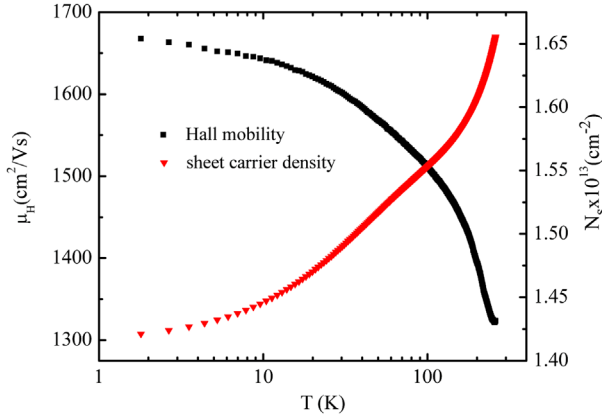


Figure 3. (colour online) Temperature dependence of the Hall mobility (μ_H) and sheet carrier density (N_s) of hole gas in the SLG/SiO₂/Si sample measured at a magnetic field of 1 T.

where w and L are the width and length of the Hall bar, e is the electronic charge and B is the applied magnetic field. μ_H and N_s were determined under a static magnetic field of 1.0 T and temperature between the 1.8 and 260 K. The temperature dependence of the μ_H and N_s in the SLG/SiO₂/Si sample is given in Figure 3. From the polarity of the V_{xy} , the type of carriers for transport is determined. The results indicate that the current flow in our sample is generated by p-type carriers and that the carrier density increases from $1.42 \times 10^{13} \text{ cm}^{-2}$ at 1.8 K to $1.65 \times 10^{13} \text{ cm}^{-2}$ at 260 K. This monotonic increment with increasing temperature in the N_s values is possibly due to thermally generated carriers. On the other hand, the μ_H of carriers in the SLG/SiO₂/Si sample was measured as $1323 \text{ cm}^2/\text{Vs}$ at 260 K, and its value increases monotonically with decreasing temperature from 260 to 1.8 K. At 1.8 K, the Hall mobility value reaches $1668 \text{ cm}^2/\text{Vs}$. This behaviour reflects the 2D character of the carriers in the single-layer graphene [16,18].

3.3. SdH oscillations and in-plane effective mass

The SdH oscillation in the magnetoresistance of a 2D system of a single-subband that is occupied is defined by the well-known Lifshitz–Kosevich formula [22], which has been used in both conventional [23–27] and Dirac-like [14,16,17,19] two-dimensional systems,

$$\frac{\Delta\rho_{xx}}{\rho_0} = f(\omega_c \tau_q) D(\chi) \exp\left[\frac{-\pi}{\mu_q B}\right] \cos\left[\frac{\pi(E_F - E_1)}{\hbar\omega_c}\right] \quad (3)$$

where $\Delta\rho_{xx}$, ρ_0 , E_F , E_1 , ω_c (eB/m^*), m^* , μ_q and τ_q are the oscillatory magnetoresistivity, zero magnetic-field resistivity, Fermi energy, first-subband energy, cyclotron frequency, effective mass, quantum mobility and quantum lifetime of 2D carriers in the first subband, respectively. The temperature dependence of the envelope function of the oscillations is contained in the function;

$$D(\chi) = \frac{\chi}{\sinh \chi} \quad (4)$$

with

$$\chi = \frac{2\pi^2 k_B T}{\hbar\omega_c} \quad (5)$$

The longitudinal resistance (R_{xx}) measurements, as a function of magnetic field for the Hall bar-shaped SLG on SiO₂/Si samples at various temperatures from 1.8 to 43 K, were performed. Magnetic fields (B) were applied perpendicular to the plane of the samples (Figure 1(b)). The current flow was in the plane of the 2D electron gas and the constant current (50 μ A) through the sample was kept low to avoid self-heating. The measured R_{xx} values for SLG on SiO₂/Si substrate for different temperatures values are shown in Figure 4. The single periodicity of the SdH oscillations is easily recognised for SLG, as shown in Figure 4. The SdH oscillations are superimposed on a rising positive non-oscillatory background magnetoresistance. The background values of the R_{xx} show much stronger magnetic field dependence. This behaviour is attributed to the parallel conduction due to the 3D carriers between the graphene layer and the SiO₂/Si substrate [13,28–33]. In our study, the graphene layers were grown on copper foil by CVD and transferred to the SiO₂/Si substrate. It is possible for residual copper atoms to remain between graphene layers and SiO₂ dielectric materials. This 3D carrier comes from the residual copper atoms between the graphene layer and SiO₂.

In order to reveal the SdH oscillations from the measured R_{xx} data, the negative second derivative ($-\frac{\partial^2 R_{xx}}{\partial B^2}$) with respect to the magnetic field of all the experimental magnetoresistance data was calculated. Figure 5 shows the results of this procedure. This technique does not change the peak position or the period of the oscillations. As seen in Figure 5, the SdH oscillations extracted from the measured R_{xx} data have well-defined envelopes and they are symmetrical about the horizontal line. In addition, the SdH oscillations have been obtained by subtracting a fitted linear function from the raw experimental data. In the low magnetic field regime ($B < 8$ T), the SdH oscillations are relatively small. For this reason,

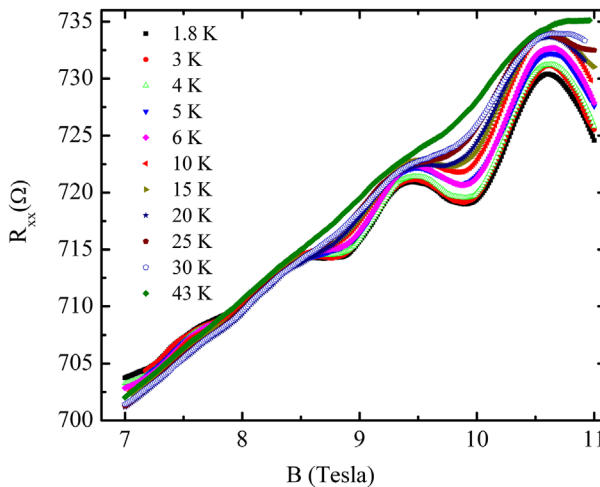


Figure 4. (colour online) Magnetoresistance (R_{xx}) as a function of the magnetic field measured at various temperature values in the SLG/SiO₂/Si sample.

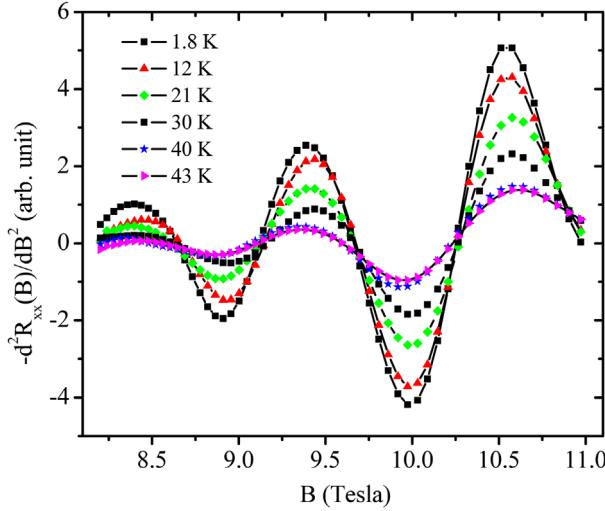


Figure 5. (colour online) Magnetic field dependence of the SdH oscillations measured at various temperature values in the SLG/SiO₂/Si sample. The full curves through the experimental data used to guide the eyes.

we did not show it in the graph. The SdH oscillations damping was measured as a function of ambient temperature. The amplitudes of the oscillations are found to be strongly damped by increasing temperature (Figure 5).

The in-plane effective mass (m^*) of 2D carriers can be extracted from the temperature dependence of the SdH amplitude at a constant magnetic field using [14,16,23,27],

$$\frac{A(T, B_n)}{A(T_0, B_n)} = \frac{T \sinh\left(\frac{2\pi^2 k_B m^* T_0}{\hbar e B_n}\right)}{T_0 \sinh\left(\frac{2\pi^2 k_B m^* T}{\hbar e B_n}\right)} \quad (6)$$

In Equation (6) the amplitudes of the oscillation peaks observed at a magnetic field B_n and at the temperatures T and T_0 are defined with the $A(T, B_n)$ and $A(T_0, B_n)$, respectively. As shown in Figure 6, the relative amplitude $A(T, B_n)$ and $A(T_0, B_n)$ decreases with increasing temperature in accordance with the usual thermal damping factor [13,14,16,23,27]. By fitting Equation (6) to the experimental data, the m^* of 2D hole gas in SLG on SiO₂/Si substrate has been determined. The m^* of 2D holes are found to be $0.0599m_0$ at a magnetic field of 9.38 T. A similar fitting process was made for all the oscillation peaks observed in the magnetic-field ranging from 8 to 11 T. In this magnetic field range, the in-plane effective mass of 2D holes is essentially independent of the magnetic field. Borghi et al. [11] has showed that the Fermi-surface effective mass in single-layer graphene sheets vanishes in the low carrier-density limit. In our study, the higher 2D carrier density ($8.13 \times 10^{12} \text{ cm}^{-2}$) in the single-layer graphene caused us to measure the non-vanishing in-plane effective mass values.

3.4. The 2D hole gas density and Fermi energy

The period of the SdH oscillations has been obtained from the plots of the reciprocal magnetic field ($1/B_n$), at which the n th peak occurs against the peak number (n). In case only one

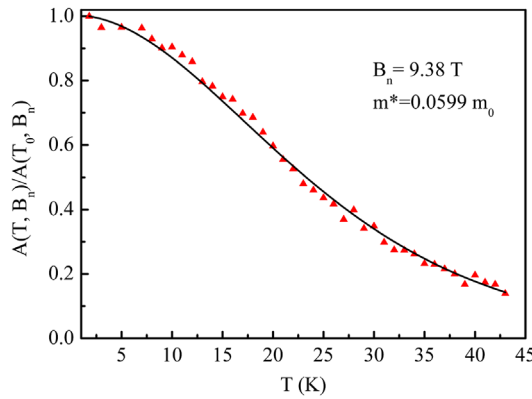


Figure 6. (colour online) Temperature dependence of the normalised amplitude of the SdH oscillation peak measured at a magnetic field of 9.38 T. The least-squares fit of Equation (6) to the experimental data is given with a full curve.

subband is occupied by hole gas, the graph of $1/B_n$ vs. n gives a straight line (Figure 7(a)), the slope of which yields the oscillation period, $\Delta(1/B)$. The Fast Fourier Transformation (FFT) of the SdH oscillations (inset of Figure 7(a)) confirm that only the first subband is populated. The Fast Fourier spectrum of the SdH oscillations for various temperatures was given in Figure 7(b). As seen in the figure, the oscillation period (hence the carrier density) is found to be essentially independent of temperature. The 2D carrier density (n_{2D}) in the SLG/SiO₂/Si sample has been calculated using the formula given in Equation (7) [14,16,23,24,27],

$$n_{2D} = \frac{g_v g_s e}{h \Delta\left(\frac{1}{B}\right)} \quad (7)$$

$$m^* = \sqrt{\frac{\pi n_{2D} \hbar^2}{V_F^2}} = \frac{E_F - E_1}{V_F^2} \quad (8)$$

In the equation, g_s , g_v are the spin and valley degeneracy and taken as two for each other in graphene materials and the e , \hbar and $E_F - E_1$ are the electric charge, Planck constant and Fermi energy with respect to the first subband energy, respectively. The n_{2D} was calculated from the period of the SdH oscillation. The effective mass and the $(E_F - E_1)$ are determined using Equation (8), where the 2D carrier density is obtained from the SdH period and $v_F = 1.1 \times 10^8$ cm/s adopted from the literature. The 2D hole gas density, effective mass and the $(E_F - E_1)$ were found to be 8.13×10^{12} cm⁻², $0.0532m_0$ and 324.19 meV at 1.8 K, respectively, and their values are essentially independent of temperature in the range from 1.8 to 43 K. A good agreement is seen between the effective mass values obtained from temperature-dependent SdH oscillation ($0.0599m_0$) and from the period of the SdH oscillations. However, the sheet carrier density, calculated from the Hall measurements, increases from 1.42×10^{13} (at 1.8 K) to 1.51×10^{13} cm⁻² (at 43 K) between the temperature range of 1.8 and 43 K. Increments in the sheet carrier density are explained as the thermal ionisation of the 3D carriers in the SiO₂/Si substrate, meanwhile concentration of the 2D carriers in the

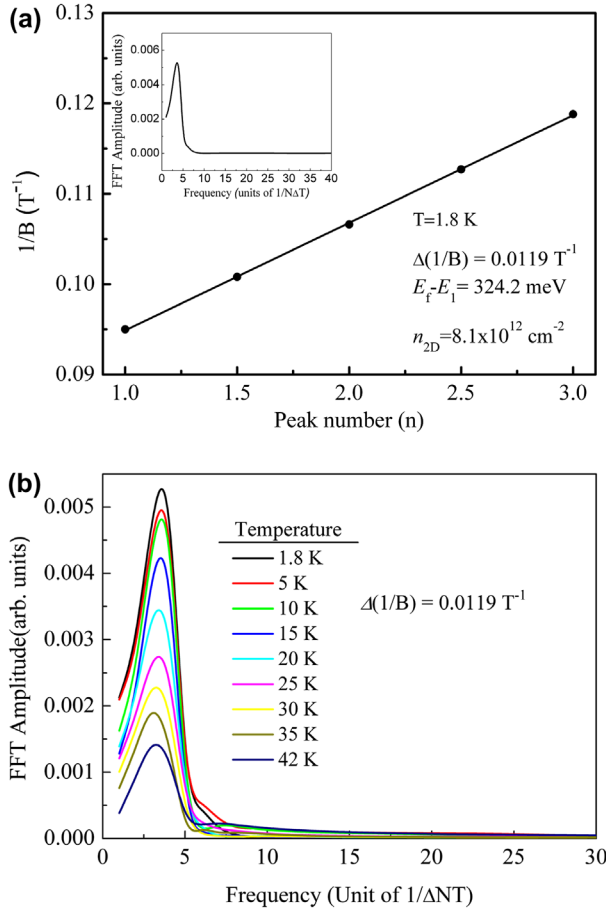


Figure 7. (colour online) (a) The reciprocal magnetic field ($1/B_n$) plotted as a function of the oscillation peak number (n). The solid line on the graph is the least-squares fit to the experimental data. The inset shows the fast Fourier spectrum of the SdH oscillations. (b) The FFT of the SdH oscillations measured at various temperatures.

SLG essentially kept constant. In our study, the sheet carrier density is larger than the 2D carrier density calculated from the SdH oscillation. The carrier density differences between two calculations methods are attributed to the bulk 3D carriers between the graphene sheet and the SiO_2/Si substrate [13,28–33].

3.5. The quantum life time of 2D carriers

The quantum life time (τ_q) is related to the Landau level broadening through $\Gamma = \hbar/2\tau_q$ induced by the potentials associated with the carrier-scattering mechanisms [13,34–38]. While τ is given by the total scattering rate, in which every scattering event is equally weighted, and is dominated by small-angle scattering, τ_t is weighted by the scattering angle and hence contains no contribution from forward scattering and only a little contribution from small-angle scattering [13,34,35]. The relationship between τ_q and the τ_t gives useful information about the nature of the complex scattering scenarios of 2D electrons (2DEGs) in the system [36,37]. For example, in the modulation-doped GaAs 2DEGs systems, the

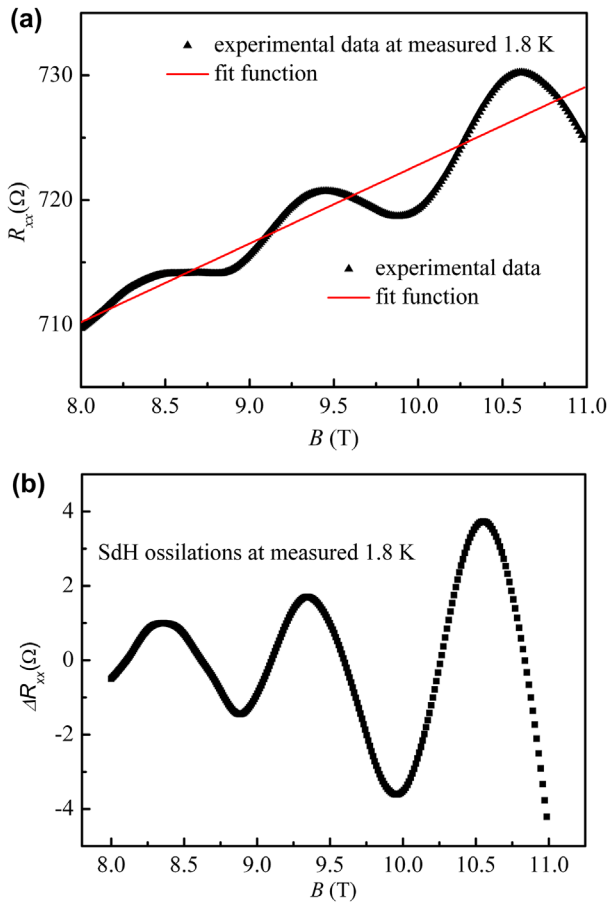


Figure 8. (colour online) (a) Measured magnetoresistance (R_{xx}) data as a function of magnetic field and linear function that fitted to the experimental data R_{xx} and (b) SdH oscillations after subtractions of the linear function from the measured R_{xx} data.

long-range nature of the scattering potential of the remote ionised impurity scattering usually results in the scattering time ratio $\tau_i/\tau_q \gg 1$. On the other hand, short-range scattering from an alloy disorder potential results in $\tau_i/\tau_q \sim 1$ [36–38]. However, in the system, when alloy scattering and ionised impurity scattering are simultaneously present, a more complicated behaviour for τ_i/τ_q would be expected.

The τ_q and τ_i are determined from the SdH oscillations and the low-field Hall Effect measurements [13,16,34]. The τ_q is one of the factors that control the envelope of the SdH oscillations. As a consequence, the quantum lifetime, and hence the quantum mobility ($\mu_q = e\tau_q/m^*$) are determined from the magnetic field dependence of the SdH oscillations amplitudes at any given constant temperature using known effective mass values [13,16,34],

$$\ln \left(\frac{A(T, B_n) \sinh \chi}{\chi} \right) = C - \frac{\pi m^*}{e \tau_q} \frac{1}{B_n} \quad (9)$$

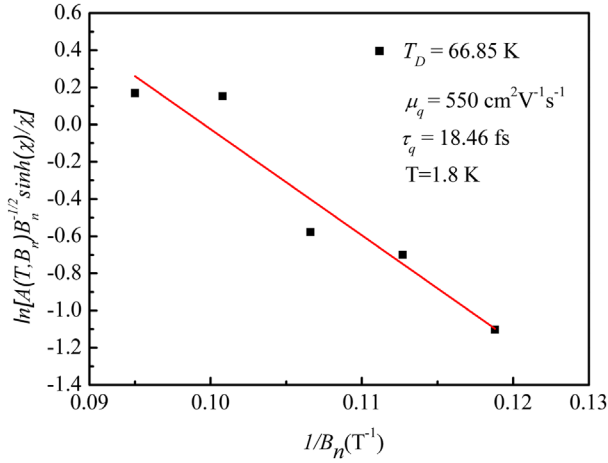


Figure 9. (colour online) Dingle plots of the SdH oscillations for obtaining the quantum lifetime of the 2D hole gas in the SLG/SiO₂/Si sample. The least-squares fit of Equation (9) to the experimental data is given with full straight lines.

The equation given above is called a Dingle plot, where $A(T, B_n)$, ω_c and C are the amplitude of the n th oscillation peak at temperature T and magnetic field B_n , cyclotron frequency and a constant, respectively. The χ is defined in Equation (5). In order to calculate Dingle temperature, quantum mobility and quantum lifetime from the Dingle plot, we calculated the $A(T, B_n)$ of the SdH oscillation from the raw data. As shown in Figure 8(a) and (b), firstly, a linear function was fitted to the measured R_{xx} values and subtracted from the R_{xx} and obtained SdH oscillations ($A(T, B_n)$).

Figure 9 shows the Dingle plots for the SLG/SiO₂/Si sample at 1.8 K. There is a good agreement between the experimental data and the straight line described by Equation (9). The linear behaviour of the experimental data indicates that the τ_q is independent of the magnetic field as assumed in Equation (9). The quantum lifetime is obtained from the slope of the Dingle plot using the values of m^* that are determined from the temperature dependence of the SdH oscillations. The Dingle temperature, quantum mobility and quantum lifetime from the Dingle plot are determined at 1.8 K as 66.8 K, 550 cm²/Vs and 18.46 fs, respectively. The measured values of T_D and μ_q are all independent of the magnetic fields and temperature in our range of measurements. In our study, the τ_t value is calculated from the low-field Hall Effect measurements as 56.80 fs. The τ_t/τ_q ratio is obtained as 3.08. The transport lifetime to quantum lifetime ratio found for SLG on SiO₂/Si substrate is consistent with the previously published data [13]. The scattering from the 3D charges, which stay between the graphene and the substrate and the source of the parallel conduction, limited the mobility of the 2D carriers in the single-layer graphene on the SiO₂/Si substrate. Recently, a systematic comparison between τ_t and τ_q has been made in the single-layer graphene sheets that mechanically exfoliated onto SiO₂/Si substrates by Hong et al. [13]. In their publications, they suggested that the mobility in the single-layer graphene on SiO₂/Si samples is limited by scattering from charges staying within 2 nm of the graphene sheet.

4. Conclusions

In the present study, the 2D carrier density, effective mass, quantum lifetime, the sheet carrier density and the transport mobility of 2D hole gas in the SLG/SiO₂/Si sample have been determined by SdH oscillations and low-field Hall effect measurements. The sheet carrier density is larger than that of the 2D carrier density calculated from the SdH oscillations. The differences between the sheet carrier density and 2D carrier density are attributed to the 3D carriers between the SL graphene and the SiO₂/Si substrate. The transport lifetime to the quantum lifetime ratio found for SLG on anSiO₂/Si substrate is 3.08.

Acknowledgements

One of the authors (E.O.) acknowledges partial support from the Turkish Academy of Sciences.

Disclosure statement

No potential conflict of interest was reported by the authors.

Funding

This work is supported by the European Union under the projects EU-METAMORPHOSE, EU-PHOREMOST, EU-PHOME, and EU-ECONAM, and TUBITAK [project number 105E066], [project number 105A005], [project number 106E198], and [project number 106A017].

References

- [1] K.S. Novoselov, A.K. Geim, S.V. Morozov, D. Jiang, Y. Zhang, S.V. Dubonos, I.V. Grigorieva, A.A. Firsov, Electric field effect in atomically thin carbon films, *Science* 306 (2004), pp. 666–669.
- [2] K.S. Novoselov, A.K. Geim, S.V. Morozov, D. Jiang, M.I. Katsnelson, I.V. Grigorieva, S.V. Dubonos, and A.A. Firsov, *Two-dimensional gas of massless Dirac fermions in graphene*, *Nature* 438 (2005), pp. 197–200.
- [3] A.H. Castro Neto, F. Guinea, N.M.R. Peres, K.S. Novoselov, and A.K. Geim, *The electronic properties of graphene*, *Rev. Mod. Phys.* 81 (2009), pp. 109–162.
- [4] D.R. Cooper, B. D’Anjou, N. Ghattamaneni, B. Harack, M. Hilke, A. Horth, N. Majlis, M. Massicotte, E. Whiteway, L. Vandsburger and V. Yu. *Experimental review of graphene*, *ISRN Condens. Matter Phys.* 2012 (2012), 56p, Article ID 501686.
- [5] L. Vicarelli, M.S. Vitiello, D. Coquillat, A. Lombardo, A.C. Ferrari, W. Knap, M. Polini, V. Pellegrini, and A. Tredicucci, *Graphene field-effect transistors as room-temperature terahertz detectors*, *Nat. Mater.* 11 (2012), pp. 865–871.
- [6] F. Bonaccorso, A. Lombardo, T. Hasan, Z. Sun, L. Colombo, and A.C. Ferrari, *Production and processing of graphene and 2d crystals*, *Mater. Today* 15 (2012), pp. 564–589.
- [7] T. Otsuji, S.A.B. Tombet, A. Satou, H. Fukidome, M. Suemitsu, E. Sano, V. Popov, M. Ryzhiiand, and V. Ryzhii, *Graphene-based devices in terahertz science and technology*, *J. Phys. D: Appl. Phys.* 45 (2012), 303001 (9pp).
- [8] F. Bonaccorso, Z. Sun, T. Hasan, and A.C. Ferrari, *Graphene photonics and optoelectronics*, *Nat. Photonics* 4 (2010), pp. 611–622.
- [9] V.P. Gusynin and S.G. Sharapov, *Magnetic oscillations in planar systems with the Dirac-like spectrum of quasiparticle excitations. II. Transport properties*, *Phys. Rev. B* 71 (2005), 125124 (8pp).
- [10] E.H. Hwang, S. Adam, and S. Das Sarma, *Carrier transport in two-dimensional graphene layers*, *Phys. Rev. Lett.* 98 (2007), 186806 (4pp).

- [11] G. Borghi, M. Polini, R. Asgari, and A.H.M. Donald, *Fermi velocity enhancement in monolayer and bilayer graphene*, Solid State Commun. 149 (2009), pp. 1117–1122.
- [12] W.A. de Heer, C. Berger, X. Wu, P.N. First, E.H. Conrad, X. Li, T. Li, M. Sprinkle, J. Hass, M.L. Sadowski, M. Potemski, and G. Martinez, *Epitaxial graphene*, Solid State Commun. 143 (2007), pp. 92–100.
- [13] X. Hong, K. Zou, and J. Zhu, *Quantum scattering time and its implications on scattering sources in graphene*, Phys. Rev. B 80 (2009), 241415(R)(4pp).
- [14] K. Zou, X. Hong, and J. Zhu, *Effective mass of electrons and holes in bilayer graphene: Electron-hole asymmetry and electron-electron interaction*, Phys. Rev. B 84 (2011), 085408 (6pp).
- [15] U. Zeitler, A.J.M. Giesbers, H.J. van Elferen, E.V. Kurganova, A. McCollam, and J.C. Maan, *Magneto-transport in the zero-energy Landau level of single-layer and bilayer graphene*, J. Phys: Conf. Ser. 334 (2011), 012035 (6pp).
- [16] E. Tiras, S. Ardali, T. Tiras, E. Arslan, S. Cakmakyapan, O. Kazar, J. Hassan, E. Janzén, and E. Özbay, *Effective mass of electron in monolayer graphene: Electron-phonon interaction*, J. Appl. Phys. 113 (2013), 043708 (8pp).
- [17] A.M.R. Baker, J.A. Alexander-Webber, T. Altebaeumer, S.D. McMullan, T.J.B.M. Janssen, A. Tzalenchuk, S. Lara-Avila, S. Kubatkin, R. Yakimova, C.-T. Lin, L.-J. Li, and R.J. Nicholas, *Energy loss rates of hot Dirac fermions in epitaxial, exfoliated, and CVD graphene*, Phys. Rev. B 87 (2013), 045414 (6pp).
- [18] E. Arslan, S. Çakmakyapan, Ö. Kazar, S. Bütün, S.B. Lişesivdin, N.A. Cinel, G. Ertaş, Ş. Ardali, E. Tıraş, J. Ul-Hassan, E. Janzén, and E. Özbay, *SiC Substrate effects on electron transport in the epitaxial graphene layer*, Electron. Mater. Lett. 10 (2014), pp. 387–391.
- [19] J. Huang, J.A. Alexander-Webber, T.J.B.M. Janssen, A. Tzalenchuk, T. Yager, S. Lara-Avila, S. Kubatkin, R.L. Myers-Ward, V.D. Wheeler, D.K. Gaskill, and R.J. Nicholas, *Hot carrier relaxation of Dirac fermions in bilayer epitaxial graphen*, J. Phys.: Condens. Matter 27 (2015), 164202 (7pp).
- [20] A.C. Ferrari, J.C. Meyer, V. Scardaci, C. Casiraghi, M. Lazzeri, F. Mauri, S. Piscanec, D. Jiang, K.S. Novoselov, S. Roth, and A.K. Geim, *Raman spectrum of graphene and graphene layers*, Phys. Rev. Lett. 97 (2006), 187401 (4pp).
- [21] R. Beams, L.G. Cançado, and L. Novotny, *Raman characterization of defects and dopants in graphene*, J. Phys.: Condens. Matter 27 (2015), 083002 (26pp).
- [22] I.M. Lifshitz and A.M. Kosevich, *Theory of magnetic susceptibility in metals at low temperatures*, Sov. Phys. – JETP 2 (1956), pp. 636–645.
- [23] T. Ando, A.B. Fowler, and F. Stern, *Electronic properties of two-dimensional systems*, Rev. Mod. Phys. 54 (1982), pp. 437–673.
- [24] I. Lo, W.C. Mitchel, R.E. Perrin, R.L. Messham, and M.Y. Yen, *Two-dimensional electron gas in GaAs/Al_{1-x}Ga_xAs heterostructures: Effective mass*, Phys. Rev. B 43 (1991), pp. 11787–11790.
- [25] J.J. Harris, J.M. Lagema, S.J. Battersby, C.M. Hellon, C.T. Foxon, and D.E. Lacklison, *Sub-band populations and the spatial distribution of electrons in GaAs/(Al, Ga)As modulation-doped quantum wells*, Semicond. Sci. Technol. 3 (1988), pp. 773–780.
- [26] S. Elhamri, A. Saxler, W.C. Mitchel, C.R. Elsass, I.P. Smorchkova, B. Heying, E. Haus, P. Fini, J.P. Ibbetson, S. Keller, P.M. Petroff, S.P. DenBaars, U.K. Mishra, and J.S. Speck, *Persistent photoconductivity study in a high mobility AlGaN/GaN heterostructure*, J. Appl. Phys. 88 (2000), pp. 6583–6588.
- [27] A. Bayraklı, E. Arslan, T. Firat, S. Özcan, Ö. Kazar, H. Çakmak, and E. Özbay, *Magnetotransport study on AlInN/(GaN)/AlN/GaN heterostructures*, Phys. Status Solidi (A) 209 (2012), pp. 1119–1123.
- [28] E.F. Schubert and K. Ploog, *Electron subband structures in selectively doped n-Al_xGa_{1-x}As/GaAs Heterostructures*, IEEE Trans. Electron Devices 32 (1985), pp. 1868–1873.
- [29] M.J. Kane, N. Apsley, D.A. Anderson, L.L. Taylor, and T. Kerr, *Parallel conduction in GaAs/Al_xGa_{1-x}As modulation doped heterojunctions*, J. Phys. C: Solid State Phys. 18 (1985), pp. 5629–5636.
- [30] F.F. Fang, T.P. Smith III, and S.L. Wright, *Landau-level broadening and scattering time in modulation doped GaAs/AlGaAs heterostructures*, Surf. Sci. 196 (1988), pp. 310–315.
- [31] S. Luryi and A. Kastalsky, *Anomalous photomagneto-resistance effect in modulation-doped AlGaAs/GaAs heterostructures*, Appl. Phys. Lett. 45 (1984), pp. 164–167.

- [32] S.J. Battersby, F.M. Selden, J.J. Harris, and C.T. Foxon, *Magnetoresistance effect in AlGaAs/GaAs two-dimensional electron gas structures at room temperature*, Solid-State Electron. 31 (1988), pp. 1083–1088.
- [33] M. van der Burgt, V.C. Karavolas, F.M. Peeters, J. Singleton, R.J. Nicholas, F. Herlach, J.J. Harris, M. van Hove, and G. Borghs, *Magnetotransport in a pseudomorphic GaAs/Ga_{0.8}In_{0.2}As/Ga_{0.75}Al_{0.25}As heterostructure with a Si δ -doping layer*, Phys. Rev. B 52 (1995), pp. 12218–12231.
- [34] P.T. Coleridge, *Small-angle scattering in two-dimensional electron gases*, Phys. Rev. B 44 (1991), pp. 3793–3801.
- [35] S. Das, *Sarma and Frank Stern, single-particle relaxation time versus scattering time in an impure electron gas*, Phys. Rev. B 32 (1985), pp. 8442–8447.
- [36] J.P. Harrang, R.J. Higgins, R.K. Goodall, P.R. Jay, M. Laviro, and P. Delescluse, *Quantum and classical mobility determination of the dominant scattering mechanism in the two-dimensional electron gas of an AlGaAs/GaAs heterojunction*, Phys. Rev. B 32 (1985), pp. 8126–8135.
- [37] A. Gold, *Scattering time and single-particle relaxation time in a disordered two-dimensional electron gas*, Phys. Rev. B 38 (1988), pp. 10798–10811.
- [38] S. Syed, M.J. Manfra, Y.J. Wang, R.J. Molnar, and H.L. Stormer, *Electron scattering in AlGaIn/GaN structure*, Appl. Phys. Lett. 84 (2004), pp. 1507–1509.